JACS
JOURNAL OF THE AMERICAN CHEMICAL SOCIETY
Article
pubs.acs.org/JACS

Motions on the Millisecond Time Scale and Multiple Conformations of HIV-1 Capsid Protein: Implications for Structural Polymorphism of CA Assemblies

In-Ja L. Byeon,[†,‡,⊥] Guangjin Hou,[†,§,⊥] Yun Han,[†,§] Christopher L. Suiter,[†,§] Jinwoo Ahn,[†,‡] Jinwon Jung,[†,‡] Chang-Hyeock Byeon,[†,‡] Angela M. Gronenborn,*[,†,‡] and Tatyana Polenova*[,†,§]

[†]Pittsburgh Center for HIV Protein Interactions and [‡]Department of Structural Biology, University of Pittsburgh School of Medicine, Pittsburgh, Pennsylvania 15261, United States

[§]Department of Chemistry and Biochemistry, University of Delaware, Newark, Delaware 19716, United States

Supporting Information

ABSTRACT: The capsid protein (CA) of human immunodeficiency virus 1 (HIV-1) assembles into a cone-like structure that encloses the viral RNA genome. Interestingly, significant heterogeneity in shape and organization of capsids can be observed in mature HIV-1 virions. In vitro, CA also exhibits structural polymorphism and can assemble into various morphologies, such as cones, tubes, and spheres. Many intermolecular contacts that are critical for CA assembly are formed by its C-terminal domain (CTD), a dimerization domain, which was found to adopt different orientations in several X-ray and NMR structures of the CTD dimer and full-length CA proteins. Tyr145 (Y145), residue two in our CTD construct used for NMR structure determination, but not present in the crystallographic constructs, was found to be crucial for infectivity and engaged in numerous interactions at the CTD dimer interface. Here we investigate the origin of CA structural plasticity using solid-state NMR and solution NMR spectroscopy. In the solid state, the hinge region connecting the NTD and CTD is flexible on the millisecond time scale, as evidenced by the backbone motions of Y145 in CA conical assemblies and in two CTD constructs (137−231 and 142−231), allowing the protein to access multiple conformations essential for pleimorphic capsid assemblies. In solution, the CTD dimer exists as two major conformers, whose relative populations differ for the different CTD constructs. In the longer CTD (144−231) construct that contains the hinge region between the NTD and CTD, the populations of the two conformers are likely determined by the protonation state of the E175 side chain that is located at the dimer interface and within hydrogen-bonding distance of the W184 side chain on the other monomer. At pH 6.5, the major conformer exhibits the same dimer interface as full-length CA. In the short CTD (150−231) construct, no pH-dependent conformational shift is observed. These findings suggest that the presence of structural plasticity at the CTD dimer interface permits pleiotropic HIV-1 capsid assembly, resulting in varied capsid morphologies.

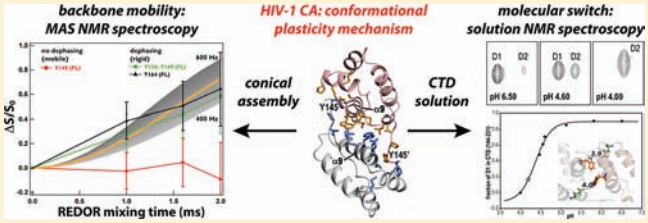

INTRODUCTION

Capsid proteins (CA) of the human immunodeficiency virus 1 (HIV-1) assemble into a cone-like structure, enclosing the viral RNA genome and a small complement of proteins during viral maturation.[1−6] Numerous electron microscopy studies on mature HIV-1 particles revealed significant heterogeneity in the appearance of capsids: a variety of shapes, such as cones, triangles, and tubes, are observed, and even virions containing multiple capsids can be detected.[7−10] As a basic model, a fullerene cone successfully explains the pleiomorphic nature of the HIV-1 capsid, comprising a hexameric CA lattice into which 12 CA pentamers are inserted to allow for closure of the ovoid.[11,12]

In solution, the N-terminal domain (NTD, ∼145 aa) exists as a monomer while the C-terminal domain (CTD, ∼90 aa) forms a dimer with a K_d value of ∼10 μM.[13−15] Full-length CA (residues 1−231) also dimerizes, albeit slightly weakly ($K_d \approx 18$ μM). Several 3D structures of both domains are available.[13,16−20] Notably, the crystal structures of the CTD dimer[14,21,22] display considerable variability at their dimerization interfaces. Crystal structures of full-length CA complexed with a Fab fragment or triiodide revealed a head-to-tail dimer[23,24] that is incompatible with the CA dimer observed in solution or in the assembled state, determined by cryo-electron microscopy (cryoEM) from tubes or flattened 2D crystal sheets.[12,13,25] Most recently, crystal structures of disulfide cross-linked, dimerization-disrupted,[26−28] hexameric, and pentameric mutant CA beautifully delineate NTD-NTD and NTD-CTD interactions in these assemblies.[29,30]

In our NMR solution structure of dimeric CTD, the side chain of Tyr145 (Y145), residue two in the polypeptide chain

Received: January 29, 2012
Published: March 19, 2012

dx.doi.org/10.1021/ja300937v | J. Am. Chem. Soc. 2012, 134, 6455−6466

(residues 144−231), was buried at the dimer interface (with only 16% solvent exposure) and engaged in extensive intersubunit interactions[13] (Figure 1A,B). Y145 was not present in

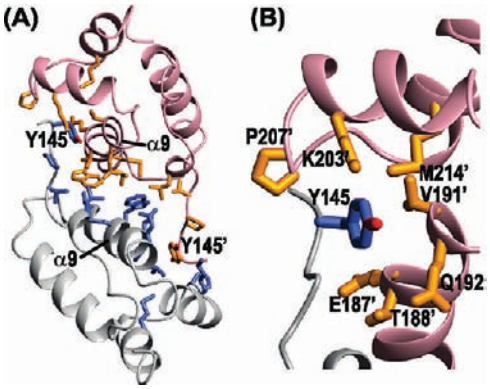

Figure 1. CTD dimer structure in solution. (A) Ribbon representation of the NMR CTD dimer structure (PDB accession code 2KOD[13]). Selected side chains at the dimer interface are shown in stick representation. One monomer unit is colored pink and orange (side chains) and the other monomer gray and blue (side chains), (B) Structural details around the Y145 side chain.

the CTD constructs used for crystallography (residues 146−231 or 151−231). Functional studies revealed a crucial role for Y145 since mutations of Y145 to Ala and Phe interfered with capsid assembly and abrogated RT activity and infectivity.[13,31] The NMR CTD dimer structure fit well into the EM density map of the assembled CA.[13] In the recent HIV capsid model,[30] the arrangement in the solution dimer (2KOD[13]) was used to connect hexamers, while the X-ray CTD dimer structure (1A43[14]) was employed to connect pentamers to hexamers, suggesting that different quaternary organization may play a role in capsid assembly.

In order to elucidate the mechanisms leading to structural polymorphism in CA capsids we conducted a combined solid-state and solution NMR study of CA, focusing on conformational dynamics of the protein.

Y145 occupies a pivotal position at the hinge between CA NTD and CTD.[31] The hinge region has been demonstrated to be a critical determinant of proper core assembly and stability.[31] We therefore analyzed the dynamic behavior of tyrosine residues in conical assemblies of full-length CA by solid-state NMR. Information about dynamics on the millisecond to nanosecond time scales can be obtained from backbone $^{13}C_{\alpha}-^{15}N$ and $^{1}H-^{15}N$ dipolar coupling constants, ^{15}N chemical shift anisotropies, and ^{15}N relaxation measurements, as demonstrated previously by us and by others.[32−35] The solid-state NMR dipolar coupling and chemical shift anisotropy data presented in this work indicate that Y145 exhibits millisecond motions in the CA proteins, while all other tyrosine residues are devoid of motions in this time regime. This millisecond time scale motion of the hinge permits the exploitation of multiple conformations in the assembly of the capsids of varied morphologies.

To examine whether different conformers are also present in solution, we investigated CTD (144−231) and CTD (150−231) and compared their behavior with full-length CA by solution NMR spectroscopy and other biophysical techniques. We show that at pH 6.5, the CTD dimer interface of the longer domain (144−231) resembles that in the full-length CA more closely than that of the shorter domain (150−231). Furthermore, at low temperature, both CTD constructs as well as full-length CA exhibit several distinct dimer conformations. Remarkably, in the long CTD (144−231) construct, the relative conformer populations are influenced by protonation−deprotonation of the E175 side chain, located at the dimer interface. This residue is within hydrogen-bonding distance of W184 on the neighboring CTD, another dimer interface residue. In contrast, in the short CTD (150−231) construct, the conformer populations are pH-invariant.

Our combined findings reveal several, slightly different conformers of CA, most likely facilitated by the intrinsic plasticity of the hinge region between NTD and CTD. The relative populations of these conformers are modulated by the protonation state of E175 located at the dimer interface that acts as a molecular switch and permits pleiotropic assembly of HIV-1 CA into capsids of different morphology.

MATERIALS AND METHODS

Protein Expression and Purification. A cDNA for the gag polyprotein, pr55^{gag}, was obtained from the NIH AIDS Research and Reference Reagent Program, Division of AIDS, NIAID, NIH.[36] Regions encoding P1-L231 (full-length CA), M144-L231 (CTD (144−231)), I150-L231 (CTD (150−231)), G137-L231 (CTD (137−231)), and V142-L231 (CTD (142−231)) were amplified and subcloned into pET21 (EMD chemicals, Inc. San Diego, CA) using *Nde*I and *Xho*I sites. Proteins were expressed in *E. coli* Rosetta 2 (DE3), cultured in Luria−Bertani or modified minimal media, after induction with 0.4 mM IPTG at 23 °C for 16 h. All proteins were purified over 5 mL Hi-Trap QP columns (GE Healthcare, Piscataway, NJ) in 25 mM sodium phosphate (pH 7.0), 1 mM DTT, 0.02% sodium azide, and 5 mL Hi-Trap SP columns (GE Healthcare, Piscataway, NJ), using a 0−1 M NaCl gradient in 25 mM sodium phosphate (pH 5.8), 1 mM DTT, 0.02% sodium azide. The final purification step comprised gel filtration over a Hi-Load Superdex 200 16/60 column (GE Healthcare) in 25 mM sodium phosphate (pH 6.5), 100 mM NaCl, 1 mM DTT, 0.02% sodium azide. Proteins were concentrated to 10 mg/mL using Amicon concentrators (Millipore, Billerica, MA), flash-frozen in liquid N_2, and stored at −80 °C. Molecular masses of purified CA proteins were confirmed by LC-TOF mass spectrometry (Bruker Daltonics, Billerica, MA). Uniform ^{15}N- and ^{13}C-labeling of the proteins was carried out by growth in modified minimal medium using $^{15}NH_4Cl$ and $^{13}C_6$-glucose as the sole nitrogen and carbon sources, respectively. Uniform ^{2}H-, ^{15}N-, and ^{13}C-labeling of the proteins was achieved using $^{2}H_2O$, $^{15}NH_4Cl$, and $^{13}C_6{}^{2}H_7$-glucose as deuterium, nitrogen, and carbon sources. For solid-state NMR experiments, full-length CA and two long CTD constructs, CTD (137−231) and CTD (142−231), were labeled with $^{13}C/^{15}N$ tyrosine by adding U-$^{13}C/^{15}N$-tyrosine prior to IPTG induction in modified minimal medium containing $^{15}NH_4Cl$ and $^{12}C_6$-glucose, as reported previously.[37]

Size-Exclusion Chromatography with In-Line Multiangle Light Scattering. Light-scattering data were obtained at room temperature using an analytical Superdex S200 column (1 cm × 30 cm) with in-line multiangle light scattering (DAWN HELEOS, Wyatt Technology, Inc., Santa Barbara, CA), refractive index (OPTILAB DSP, Wyatt Technology, Inc.), and UV (Agilent Technologies, Santa Clara, CA) detectors. First, 100 μL of the CTD (144−231) and CTD (150−231) proteins at two different concentrations were applied to the pre-equilibrated S200 column and then were eluted with 25 mM sodium phosphate buffer, pH 6.5, 0.02% sodium azide, 1 mM DTT at a flow rate of 0.5 mL/min.

Isothermal Titration Calorimetry (ITC). Heats of dissociation of the CTD (144−231) and (150−231) dimers were measured following established protocols[38,39] using a VP-ITC instrument (MicroCal Inc.). All samples were extensively buffer exchanged using Amicon concentrators (Millipore, Billerica, MA) prior to the experiments. Typically, 3-μL aliquots of 0.816 mM CTD (144−231) or 1.009 mM

CTD (150−231) protein solution were injected to the cell at 17 °C, containing 1.413 mL of 25 mM sodium phosphate buffer, pH 6.5, 0.02% azide, 1 mM TCEP with stirring at 307 rpm followed by 35 subsequent injections of 4-μL aliquots. Injections were performed in 250 s intervals with an initial delay of 60 s. Dilution heats were obtained by injecting buffer into the cell containing the same buffer and used for correction to extract true dissociation heats. The K_d values were determined by curve fitting[38,39] with Origin 7 software (OriginLab Corp.) implemented in MicroCal ITC routines (MicroCal Inc.), using a dimer-to-monomer model.

Solution NMR Spectroscopy. All NMR spectra were recorded at temperatures ranging from 7 to 42 °C for samples containing 0.44−2.6 mM $^{13}C/^{15}N$-labeled CTD (144−231), CTD (150−231), and $^{2}H/^{13}C/^{15}N$-labeled full-length CA in 25 mM sodium phosphate buffer, pH 6.5, 0.02% azide, 5−10 mM DTT on Bruker AVANCE 900, 800, 700, and 600 spectrometers, equipped with 5 mm triple-resonance, *z*-axis gradient cryoprobes. Probe temperatures were calibrated with 100% methanol using the chemical shift difference between methyl and hydroxyl protons.[40] Backbone and C_β resonance assignments of CTD (150−231) at 7 °C were carried out using heteronuclear 2D $^{1}H-^{15}N$ HSQC and 3D HNCACB, HN(CO)-CACB, HNCA, and HN(CO)CA experiments.[41,42] A 3D simultaneous ^{13}C- and ^{15}N-edited NOESY[43,44] experiment at 7 °C with a mixing time of 100 ms was employed to confirm the assignments from the heteronuclear multidimensional NMR data. T186 $^{15}N-^{1}H$ auto and exchange peak intensities were used to calculate the exchange rate between the D1 and D2 dimers, utilizing the equation 9.1.5 in Ernst et al.[45] for a symmetrical two-site system.

pH titration experiments of CTD (144−231) and (150−231) were conducted at 600 MHz, 7 °C by obtaining $^{1}H-^{15}N$ HSQC at pH range between 6.5 and 4.0. The pK_a value of E175 in CTD (144−231) at 7 °C was determined from the fitting of the D1 fraction (monitored by nearby W184 $N_{\varepsilon 1}H$ peak) vs pH titration curve to a modified Hill equation[46] by nonlinear least-squares analysis:

$$\text{fraction}_{obs} = (\text{fraction}_{A^-} + \text{fraction}_{AH}10^{n(pK_a-pH)}) / (1 + 10^{n(pK_a-pH)})$$

where fraction_{obs} is the D1 fraction observed at each pH value, fraction_{A^-} and fraction_{AH} are the D1 fractions with completely deprotonated and protonated E175, respectively, and n is a Hill coefficient. Curve fits were performed using the KaleidaGraph4.0 Software (Synergy Software), and the best-fit values for pK_a, fraction_{A^-}, fraction_{AH}, and n are reported here.

Spectra were processed with NMRPipe[47] and analyzed using SPARKY3 (version 3.115)[48] and NMRView.[49]

Solid-State NMR Spectroscopy. CA samples for solid-state NMR experiments were in 25 mM sodium phosphate buffer, pH 5.5, 1 mM DTT, 0.02% NaN_3. Conical assemblies were prepared by adding a 20% w/v solution of PEG-20000 to 32 mg/mL U-$^{13}C/^{15}N$-tyrosine-labeled CA protein in a 1:1 ratio, followed by incubation at 37 °C for 1 h, as reported previously.[50] The morphology was evaluated by negatively stained TEM and confocal microscopy. CTD (137−231) and CTD (142−231) samples were prepared by controlled precipitation with PEG 3350, by adding a 60% w/v solution of PEG 3350 to 32 mg/mL protein in a 1:1 ratio. Samples were pelleted by centrifugation at 6000*g* for 15 min, the supernatant was removed, and 15 mg (0.59 μmol) portions of full-length conical CA assemblies were packed into 3.2 and 1.8 mm MAS rotors. Next, 17 mg (1.61 μmol) of CTD (137−231) and 18.5 mg (1.83 μmol) of CTD (142−231) were packed into two 1.8 mm rotors. The rotors were sealed using an upper spacer and a top spinner for subsequent MAS NMR experiments.

All solid-state NMR experiments were carried out on a 14.1 T narrow bore Varian InfinityPlus solid-state NMR spectrometer operating at Larmor frequencies of 599.8, 150.8, and 60.8 MHz for ^{1}H, ^{13}C, and ^{15}N, respectively. All solid-state NMR spectra of U-$^{13}C/^{15}N$-tyrosine-labeled capsid assemblies were obtained with a 3.2 mm Varian triple-resonance T3 probe, with the exception of the ^{15}N ROCSA chemical shift anisotropy (CSA) recouping spectra. The ROCSA spectra of the full-length capsid assemblies and all spectra of the CTD samples were acquired with a 1.8 mm MAS triple-resonance probe developed in the Samoson laboratory. The MAS frequency was set at 10 kHz for all NMR experiments and was controlled to within ±2 Hz by a Varian MAS controller. PbNO3 was used as temperature sensor to calibrate the sample temperature in both MAS NMR probes.[51] The actual temperature of the sample was maintained to within ±0.1 °C using the Varian temperature controller and was set to the desired value over the range of 238 to 288 K. All CP, $^{1}H-^{15}N$ dipolar, ^{15}N CSA, and $^{15}N\{^{13}C\}$ REDOR spectra were collected at 258 K. ^{13}C and ^{15}N chemical shifts were referenced with respect to the external standards adamantane and ammonium chloride, respectively.[52]

Intraresidue assignments of tyrosine resonances were obtained using 1D ^{15}N and ^{13}C CP/MAS as well as 2D homonuclear $^{13}C-^{13}C$ DARR and $R2_1^1$ experiments,[53,54] and heteronuclear $^{13}C-^{15}N$ NCA experiment. For H−X (X = ^{13}C or ^{15}N) cross-polarization (CP), a linearly ramped rf field and a constant-amplitude rf field were applied on the X nucleus and on ^{1}H, respectively. For the NCA experiments, SPECIFIC-CP[55] with a tangent amplitude ramp was used for band selective magnetization transfer from ^{15}N to ^{13}C. All CP and SPECIFIC-CP conditions were optimized experimentally to attain the first-order Hartmann−Hahn matching condition.

In the 2D DIPSHIFT[56] and ^{15}N CSA recoupling experiments, rotor-synchronized $R18_1^7$ symmetry[57] and ROCSA[58] blocks were incorporated during the t_1 period for $^{1}H-^{15}N$ dipolar and ^{15}N CSA evolution, respectively. The radio frequency field strength applied on the ^{1}H channel during the $R18_1^7$ period was 90 kHz, and that applied on the ^{15}N channel during the ROCSA period was 42.8 kHz. A $^{15}N\{^{13}C\}$ rotational echo double resonance (REDOR) experiment[59] was conducted to assess the $^{13}C_\alpha$-^{15}N dipolar coupling constants for each tyrosine residue in the three protein samples. A series of REDOR spectra were recorded with mixing times of 1.0, 1.6, and 2.0 ms. A 1D CA-N experiment was performed on the full-length conical CA assemblies, whereas SPECIFIC-CP with a tangent amplitude ramp was used to achieve the band-selective magnetization transfer from $^{13}C_\alpha$ to ^{15}N. All solid-state NMR data were processed with NMRPipe[47] and analyzed with SPARKY3 (version 3.115).[48]

Analysis and Simulations of Solid-State NMR Spectra. Numerical simulations of $^{1}H-^{15}N$ dipolar and ^{15}N CSA spectra as well as of $^{15}N\{^{13}C\}$ REDOR dipolar dephasing curves were performed with the SIMPSON software package.[60] A total of 986 pairs of $\{\alpha,\beta\}$ angles generated according to the ZCW algorithm[61] and 64 γ angles (resulting in a total of {63,104} angle triplets) were used to generate a powder average for all simulations. For extracting the best-fit dipolar (ω_D) and CSA parameters (δ_σ, η_σ), all the experimental and processing parameters (i.e., Larmor frequency, MAS frequency, RF field strength, number of t_1 points, finite pulse lengths, zero-filling, line broadening, etc.) were taken into account in the simulations for each experiment.

CSA Tensor Convention. We use the Haeberlen convention in which the CSA tensor is characterized by three parameters, isotropic chemical shift (δ_{iso}), reduced anisotropy (δ_σ), and asymmetry parameter (η_σ).[62] These parameters are defined in terms of the principal components of the CSA tensor, with the isotropic chemical shift as $\delta_{iso} = (\delta_{11} + \delta_{22} + \delta_{33})/3$. The reduced anisotropy (δ_σ) and the asymmetry parameter (η_σ) are defined as $\delta_\sigma = \delta_{11} - \delta_{iso}$ and $\eta_\sigma = (\delta_{22} - \delta_{33})/\delta_\sigma$ if $|\delta_{11} - \delta_{iso}| \geq |\delta_{33} - \delta_{iso}| \geq |\delta_{22} - \delta_{iso}|$ (positive anisotropy), or $\delta_\sigma = \delta_{33} - \delta_{iso}$ and $\eta_\sigma = (\delta_{22} - \delta_{11})/\delta_\sigma$ if $|\delta_{33} - \delta_{iso}| \geq |\delta_{11} - \delta_{iso}| \geq |\delta_{22} - \delta_{iso}|$ (negative anisotropy). The asymmetry parameter ranges from 0 to 1.

RESULTS AND DISCUSSION

Tyr-145 Exhibits Millisecond Time Scale Mobility in the Assembled CA and in the CTD. It has been previously postulated that the likely origin for structural polymorphism of CA capsids may be the inherent flexibility of the hinge region between NTD and CTD, making multiple, slightly different local structures available for assembly.[21,24] To test this

hypothesis we employed magic angle spinning solid-state NMR spectroscopy on $^{13}C/^{15}N$-tyrosine-labeled CA conical assemblies and probed the backbone dynamics on multiple time scales spanning nano- to millisecond range. For comparison, we also investigated two $^{13}C/^{15}N$-tyrosine-labeled CTD constructs (CTD (137−231) and CTD (142−231)) prepared as hydrated nanocrystals. These CTD constructs are slightly longer than the CTD (144−231) used in solution NMR studies (see below), since we were concerned that truncating the N-terminal portion of CA too close to the hinge may introduce additional artificial conformational flexibility that could affect the interpretation of the backbone dynamics results. For these two CTD constructs (CTD (137−231) and CTD (142−231)), solution $^{1}H-^{15}N$ HSQC spectra acquired at 280 K (shown in the Supporting Information, Figure S1) reveal that the relative populations of D1 and D2 conformers are similar to those for the CTD (144−231) protein (vide infra).

The CA protein contains four tyrosine residues, one located in the NTD (Y130), two in the CTD (Y164 and Y169), as well as the critical residue Y145 located around the hinge region. Therefore, focusing on the backbone atoms of these tyrosine residues permits assessment of the dynamics behavior in each domain and the hinge region. For Y130, Y164, and Y169, ^{13}C and ^{15}N chemical shift assignments were available from our prior solid-state and solution NMR studies,[50,63] and therefore residue-specific isotopic labeling was selected for the MAS NMR dynamics investigation. For Y145, ^{15}N and $^{13}C_{\alpha}$ chemical shifts were assigned by comparing the ^{15}N and ^{13}C CPMAS spectra of full-length CA in conical assemblies with those of the two CTD constructs. As depicted in Figure 2, Y145 gives rise to

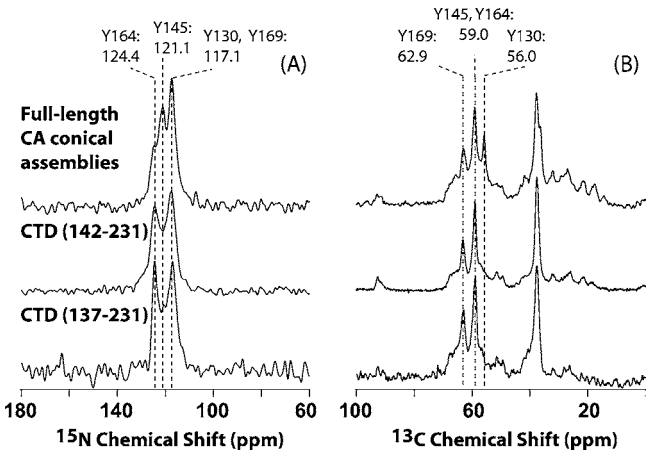

Figure 2. (A) ^{15}N CPMAS spectra of full-length CA conical assemblies (top), CTD (142−231) (middle), and CTD (137−231) (bottom). (B) ^{13}C CPMAS spectra of full-length conical CA assemblies (top), CTD (142−231) (middle), and CTD (137−231) (bottom). Resonance assignments are provided and were confirmed in 2D $^{13}C-^{13}C$ and $^{15}N-^{13}C$ correlation spectra. The solid-state NMR chemical shifts agree well with those from solution NMR.

a well-resolved peak in the ^{15}N CPMAS spectra of CA conical assemblies (121.1 ppm). Interestingly, the corresponding peak is broadened in the spectra of the CTDs, either due to conformational heterogeneity or internal backbone motion on the time scales of the cross-polarization, or both. In the ^{13}C CPMAS spectra, the Y145 $^{13}C_{\alpha}$ peak overlaps with the Y164 resonance (59.0 ppm).

In order to resolve the chemical shift degeneracy for Y130/Y169 ^{15}N and Y145/Y169 $^{13}C_{\alpha}$ resonances, two-dimensional homonuclear $R2_1^1$ $^{13}C-^{13}C$ and heteronuclear NCA spectra were acquired on all three protein samples. The $R2_1^1$ spectrum for the CTD (142−231) reveals strong aliphatic-to-aliphatic and carbonyl-to-aliphatic correlations for Y164 and Y169 residues in the CTD (142−231) sample (Figure 3A), while

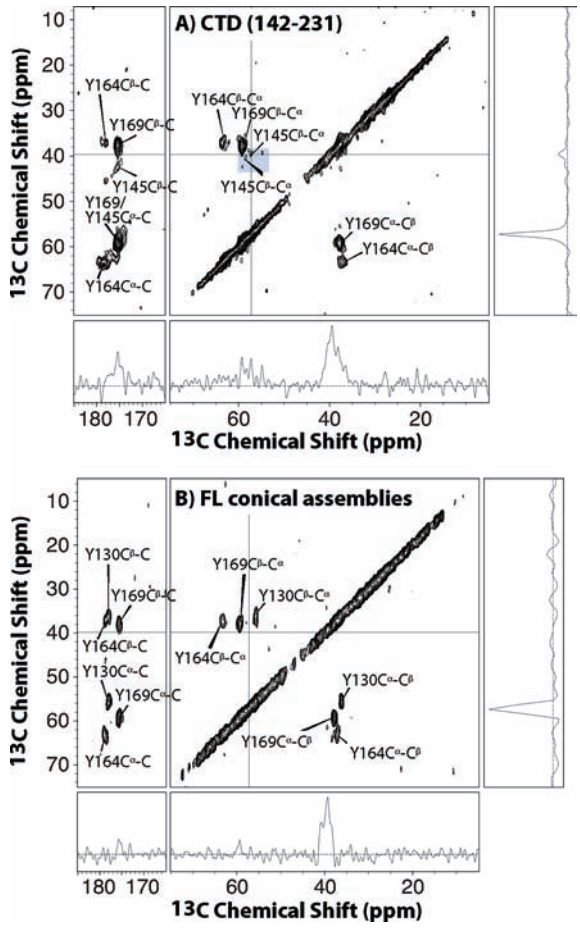

Figure 3. $^{13}C-^{13}C$ $R2_1^1$ correlation spectra of CTD (142−231) (A) and full-length conical CA assemblies (B) for the aliphatic and carbonyl regions. 1D slices extracted along the ω_2 and ω_1 frequency dimensions are shown to illustrate that weak cross peaks corresponding to the different Y145 conformers are clearly above the noise level in the CTD (142−231) spectra. No Y145 resonances were detected for full-length CA assemblies.

Y145 exhibits multiple C_{α}-C_{β} cross peaks that are weak, but distinctly above the noise level (see the 2D contour plot and the 1D slice extracted along the ω_2 frequency dimension). This suggests that Y145 is conformationally heterogeneous in the CTD (142−231). The $R2_1^1$ spectrum of full-length CA conical assemblies exhibits strong cross peaks for Y130, Y164, and Y169, with no correlations detectable for Y145. The most likely reason for detecting Y145 correlations in the C−C spectra of CTD (142−231), but not in full-length CA is that we were able to pack more protein into the rotor and therefore the inherent sensitivity of all NMR experiments was higher for CTD (142−231) (see Figure 2). We also note that the solution $^{1}H-^{15}N$ HSQC spectrum of U-$^{13}C/^{15}N$-tyrosine labeled full-length CA only contains the Y130 amide resonance, while those of Y145, Y164, and Y169 are broadened beyond detection (see Figure

dx.doi.org/10.1021/ja300937v | J. Am. Chem. Soc. 2012, 134, 6455−6466

S2 of the Supporting Information), precluding solution NMR studies of tyrosine dynamics in dimeric unassembled CA.

For all three proteins, cross peaks for the N−C_α correlation of Y145 are missing in the NCA spectra (Figure 4), suggesting

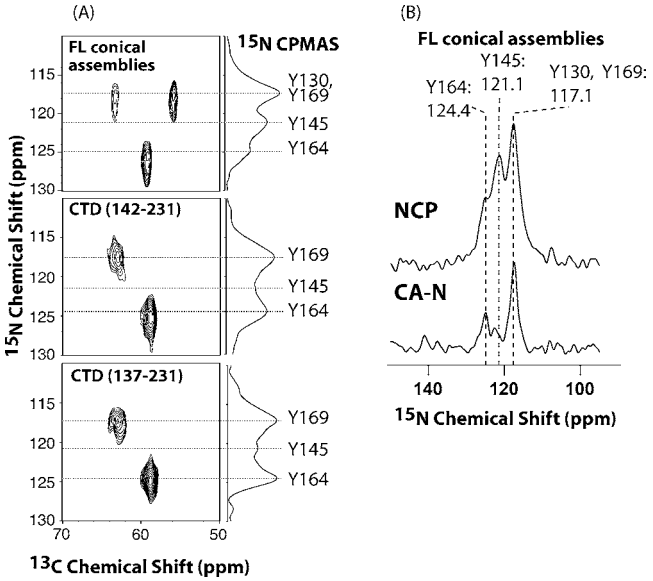

Figure 4. (A) Two-dimensional NCA spectra of full-length conical CA assemblies (top), CTD (142−231) (middle), and CTD (137−231) (bottom) at 258 K. On the right, the corresponding 1D ^{15}N CPMAS spectra are displayed. Note that the Y145 peak is present in all ^{15}N CPMAS spectra, while Y145 cross peaks are missing in the 2D NCA spectra, suggesting that the ^{15}N−^{13}C dipolar couplings are motionally averaged. (B) CA-N (bottom) and ^{15}N CPMAS (top) spectra of full-length CA conical assemblies, illustrating that the Y145 peak intensity is severely attenuated in the CA-N data, most likely due to motional averaging of the corresponding ^{15}N−^{13}C dipolar coupling.

that motion on the millisecond time scale is present for the backbone atoms at position 145, causing motional averaging of the N−C_α dipolar coupling (the rigid limit ω_D = 984 Hz). In an attempt to recover the Y145 cross peak, we collected a series of NCA spectra for temperatures between +5 °C and −35 °C; unfortunately, this temperature range is too narrow to push the motional rates from the intermediate into either the fast or the slow regime (Figure S3 in Supporting Information). The notion that motional averaging of the Y145 N−C_α dipolar coupling causes the loss of the Y145 cross peak in the NCA spectra is corroborated by a complementary 1D CA-N experiment (Figure 4B): the intensity of the Y145 resonance is severely attenuated, in contrast to the intensities of the Y130/Y169 and Y164 resonances.

For all remaining tyrosine residues, strong cross peaks that are temperature independent are observed in the NCA spectra.

To assess the extent of motional averaging of the Y145 N−C_α dipolar coupling in full-length CA conical assemblies and CTDs, ^{15}N{^{13}C} REDOR dephasing curves were acquired. The dephasing profiles for Y130, Y164, and Y169 in the full-length CA assemblies (and for Y164 and Y169 in the two CTDs) are indistinguishable within the experimental error (Figure 5), and the corresponding ^{15}N−$^{13}C_\alpha$ dipolar couplings extracted from the curves are 500 ± 200 Hz, slightly lower than the rigid limit value of 984 Hz. In contrast, the Y145 ^{15}N−$^{13}C_\alpha$ dipolar coupling is completely averaged to zero and undetectable within the experimental error (no dipolar dephasing is observed, Figure 5), indicating the presence of motions on a time scale of 10 ms or faster.

Tyr-145 Is Rigid on Time Scales Faster than Milliseconds in the Assembled CA and in the CTD. Having determined that the slow limit for the Y145 backbone motion is on the time scale of 10 ms or faster, we next investigated whether motions on the micro- to nanosecond time scales can be detected by probing ^{1}H−^{15}N dipolar and ^{15}N chemical shift anisotropy.

^{1}H−^{15}N dipolar line shape measurements using the 2D ^{15}N-detected $R18_1^7$ sequence for full-length CA assemblies and the two CTDs (Figure 6), revealed strikingly similar ^{1}H−^{15}N dipolar coupling constants, ω_D, for all tyrosine residues in all the three samples. The couplings were extracted from the dipolar line shapes by numerical simulations and are only slightly smaller than the rigid limit value of 11.8 kHz, with dipolar order parameters ranging from 0.84 to 0.91 for Y145 and from 0.88 to 0.93 for the remaining tyrosines. Furthermore, the dipolar line shapes are consistent with an axial dipolar tensor, another indication that the H−N bond vector is rigid or close to being rigid for times faster than ca. 80 μs. Interestingly, variations in the fine structure of the dipolar line shapes can be seen, notably, in intensities of the center peaks (determined by ^{1}H CSA and relaxation), reporting on small differences in local structure around the corresponding H−N bond vectors.

^{15}N chemical shift anisotropies for all Tyr backbone atoms were probed by 2D ^{15}N-detected ROCSA experiments (Figure 7). Since the rigid-limit ^{15}N reduced chemical shift anisotropy value (δ_σ = 110 ppm corresponding to the full CSA interaction strength of 165 ppm or 10.0 kHz at 14.1 T) is similar to the rigid-limit value of the ^{1}H−^{15}N dipolar coupling (11.8 kHz), both interactions are sensitive to motions on the same time scales, namely micro- to nanoseconds. In agreement with our findings for the ^{1}H−^{15}N dipolar line shapes, the ^{15}N CSA tensor parameters, δ_σ and η_σ are strikingly similar for all tyrosine residues in all samples. For the full-length conical CA assemblies and the two CTD samples, δ_σ values for all Tyr residues are close to the rigid limit value. The asymmetry parameters, η_σ, are also similar and lie between 0.20 and 0.36, indicating that the CSA tensors are close to being axially symmetric. Therefore, taken together, the ^{1}H−^{15}N dipolar and ^{15}N CSA results indicate that the backbone atoms of all tyrosine residues, including Y145, are rigid or mostly rigid on the microsecond or faster time scales.

The backbone dynamics data of Y145 in conically assembled CA, extracted from REDOR, ^{1}H−^{15}N dipolar, and ^{15}N CSA MAS NMR experiments, clearly indicate motions in the millisecond regime. These millisecond time scale motions in the hinge region detected by MAS solid-state NMR define the conformational space of CA with multiple conformations in principle accessible for the assembly into capsids of different morphologies.

CTD (150−231) and CTD (144−231) Exhibit Slightly Different Dimerization Affinity in Solution. To examine whether different CA conformers exist in solution and if there are distinct conformational preferences that could explain its assembly into pleiomorphic conical capsids in the virus, we conducted combined biophysical/solution NMR analyses of two CTD constructs ((144−231) and (150−231)) and a full-length CA. CTD (146−231) and CTD (144−231) proteins have been reported to dimerize with essentially the same affinity with reported K_d values of 10 ± 3 μM[13] and 9.8 ± 0.6 μM,[14] respectively. The K_d value of the shorter CTD construct

dx.doi.org/10.1021/ja300937v | J. Am. Chem. Soc. 2012, 134, 6455−6466

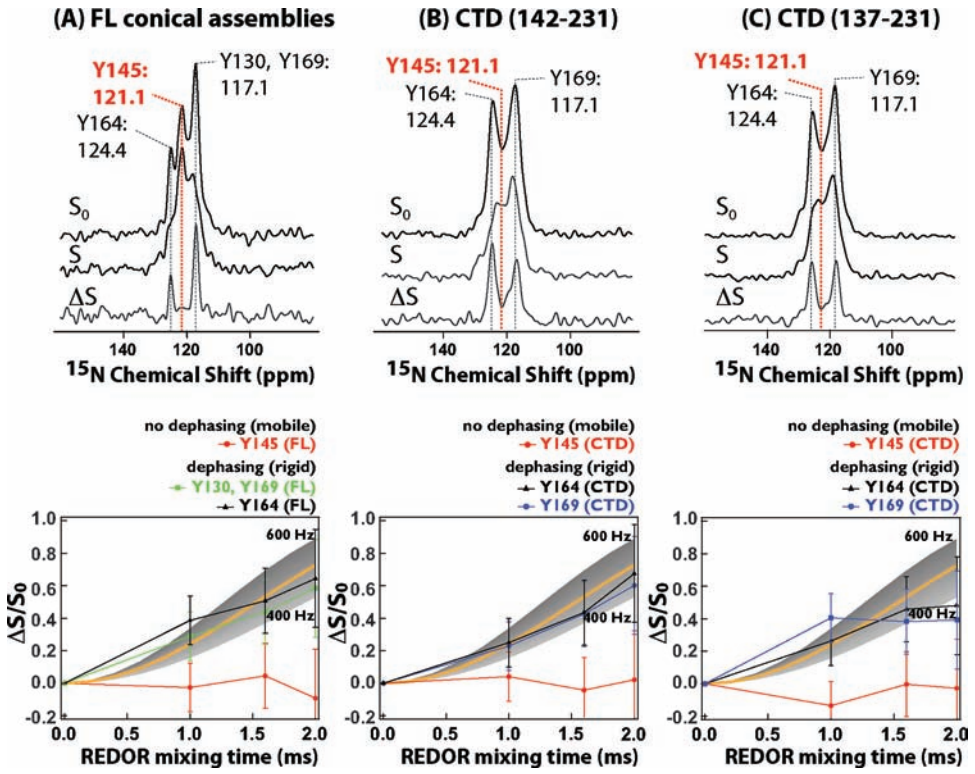

Figure 5. $^{15}N\{^{13}C\}$ REDOR spectra (top) and dephasing curves (bottom) of (A) full-length CA conical assemblies, (B) CTD (142−231), and (C) CTD (137−231). In the REDOR spectra, S_0 and S are the peak intensities in the absence and presence of REDOR dephasing pulses, respectively. $\Delta S = S_0 - S$ is the intensity difference. In the REDOR dephasing curves, the REDOR fraction, $\Delta S/S_0$, is plotted against the mixing time. Note that for all three proteins, Y145 does not exhibit REDOR dephasing, caused by motional averaging of the $^{15}N-^{13}C$ dipolar coupling on the time scale of the REDOR experiment (~10 ms).

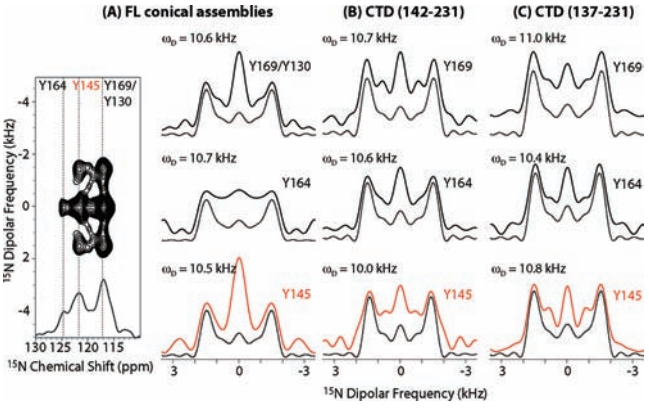

Figure 6. $^{1}H-^{15}N$ dipolar line shapes for tyrosine residues in (A) full-length CA conical assemblies, (B) CTD (142−231), and (C) CTD (137−231). For full-length assembled CA, the 2D $^{1}H-^{15}N$ DIPSHIFT spectrum is shown to illustrate the high quality of the data. Experimental dipolar line shapes and the best-fit line shapes are shown in solid lines and dashed lines, respectively. The experimental line shapes for Y145 are highlighted in red. For each residue, the $^{1}H-^{15}N$ dipolar coupling constant, ω_D, extracted by numerical simulations, is listed. Note that all tyrosine residues exhibit essentially rigid-limit behavior on the time scale of the DIPSHIFT experiment.

(residues 150−231) was qualitatively assessed by multiangle light scattering (SEC-MALS) and compared with CTD (144−231).[13] Loading a 1.15 mM CTD (144−231) solution (100 μL) onto the Superdex 200 column yielded a weight-averaged molecular mass of 18.1 kDa that was reduced to 16.3 kDa upon 5-fold dilution solution (Figure 8A). The equivalent values obtained for CTD (150−231), loading 0.77 mM and 0.15 mM (100 μL), were 16.3 kDa and 14.3 kDa, respectively (Figure 8B). Thus, CTD (150−231) exhibits a slightly lower averaged mass upon dilution than CTD (144−231), suggesting that the

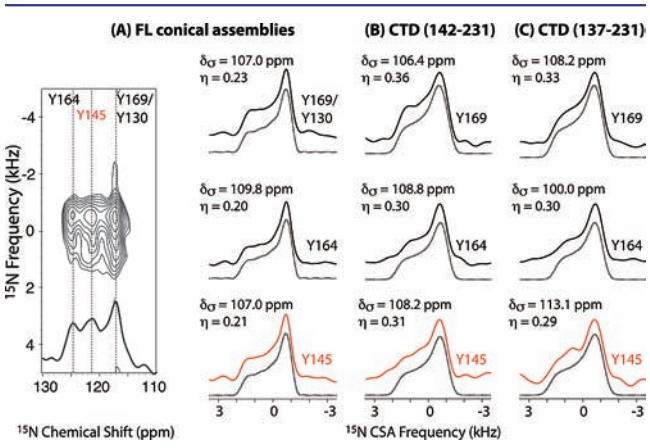

Figure 7. ^{15}N CSA line shapes for tyrosine residues in (A) full-length CA conical assemblies, (B) CTD (142−231), and (C) CTD (137−231). For full-length CA, the 2D ^{15}N ROCSA spectrum is shown to illustrate the high quality of the data. Experimental and best-fit CSA line shapes are shown in solid and dashed lines, respectively. The experimental line shapes for Y145 are highlighted in red. For each residue, the ^{15}N CSA tensor parameters, δ_σ and η_σ, extracted by numerical simulations, are listed. Note that all tyrosines residues exhibit essentially rigid-limit parameters *o*n the time scale of the ROCSA experiment.

dx.doi.org/10.1021/ja300937v | J. Am. Chem. Soc. 2012, 134, 6455−6466

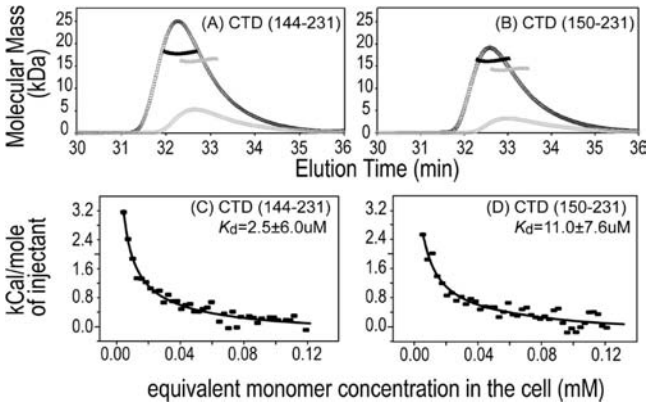

Figure 8. SEC-MALS and ITC of CTD (144−231) and CTD (150−231). (A,B), 100 μL each of 1.15 mM (black) and 0.23 mM (gray) CTD (144−231) and of 0.77 mM (black) and 0.15 mM (gray) CTD (150−231), respectively, were applied to the S200 column. The predicted molecular masses (filled triangles) and the elution profiles (open circles) are shown as a function of the elution time. (C,D) Dimer dissociation measured by ITC: dissociation isotherms corrected for dilution heats and the best fit to a dimer−monomer dissociation model to the experimental data is depicted by a solid line.

shorter CTD (150−231) dimer is slightly weaker than the longer CTD.

Dimer dissociation constants for CTD (144−231) and (150−231) were quantitatively measured by ITC, yielding K_d values of 2.5 ± 6.0 μM and 11.0 ± 7.6 μM, respectively (Figure 8C,D). These values are similar to the K_d value for CTD (144−231), reported previously from NMR (~10 μM).

CTD (150−231) and CTD (144−231) Exhibit Differences at Their Dimer Interfaces. ^{1}H−^{15}N HSQC spectra of CTD (144−231) and (150−231) at 900 MHz and 25 °C (Figure 9) using protein concentrations for which ≥95% of the protein is dimeric (2.0 mM for 144−231 CTD and 2.6 mM for the 150−231 CTD) revealed distinct differences for resonances

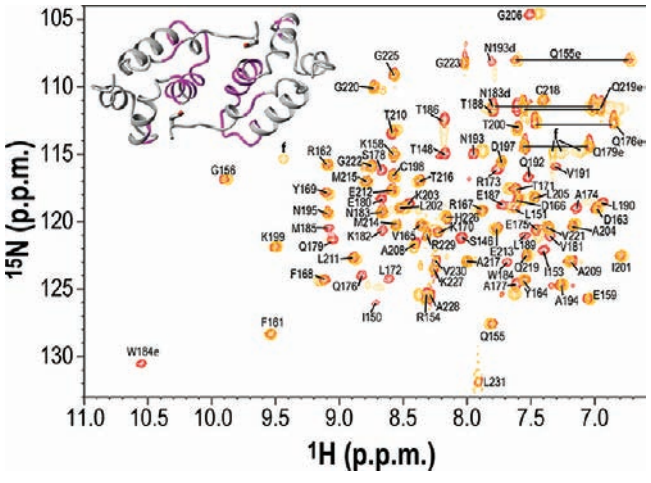

Figure 9. Superposition of the 900 MHz ^{1}H−^{15}N HSQC spectra of the CTD (144−231) (red, 2 mM, pH 6.5) and CTD (150−231) (orange, 2.6 mM, pH 6.5) at 25 °C. Amide resonances are labeled by residue name and number, and several side-chain resonances are also labeled. A few folded side-chain resonances are labeled with the letter "f". Inset, structural mapping of the broadened/missing resonances for the shorter CTD (150−231) (colored magenta) onto the NMR CTD (144−231) dimer structure.[13].

associated with residues at the dimer interface. In the spectrum of CTD (150−231), amide resonances of S178, E180, V181, K182, W184, and M185 are missing. They all belong to helix α9, the central dimerization helix. In addition, amide resonances of I153, R154, L172, R173, A174, E175, Q176, A177, Q179, T186, E187, L189, L190, V191, Q192, N193, K203, and G206 are also severely line-broadened or exhibit slightly different resonance frequencies from those reported previously for the longer CTD (144−231).[13,63] All affected residues (broadened or shifted) for CTD (150−231) are mapped onto the NMR CTD (144−231) dimer interface[13] (inset in Figure 9). Although interfacial residues for CTD (144−231) also exhibit some broadening, this is significantly less and all resonances, but one, were observed.[13] The line broadening varies with the magnetic field strength. For example, the W184 $N_{\varepsilon 1}H$ and R173 backbone NH resonances of CTD (150−231) that are broadened beyond detection at 900 MHz are clearly observable at 600 MHz (Figure S4 of the Supporting Information), demonstrating that broadening is caused by chemical exchange.

Full-Length CA Exhibits a CTD Dimer Conformation More Similar to That of CTD (144−231) than CTD (150−231). High-quality ^{1}H−^{15}N HSQC spectra of full-length CA have been difficult to obtain up to now, not because of large molecular size of the protein, but primarily since conformational exchange accompanies dimerization and results in a heterogeneous dimer interface of the protein.[13,64] In addition, full-length CA exhibits nonspecific aggregation at high concentrations (≥1 mM), resulting in poor spectra (Figure S5 in the Supporting Information). Fortunately, using 0.87 mM ^{2}H/^{15}N/^{13}C-triply isotopically labeled protein yielded an acceptable quality ^{1}H−^{15}N HSQC spectrum (Figure 10) that could be compared with spectra of CTD (144−231) and CTD

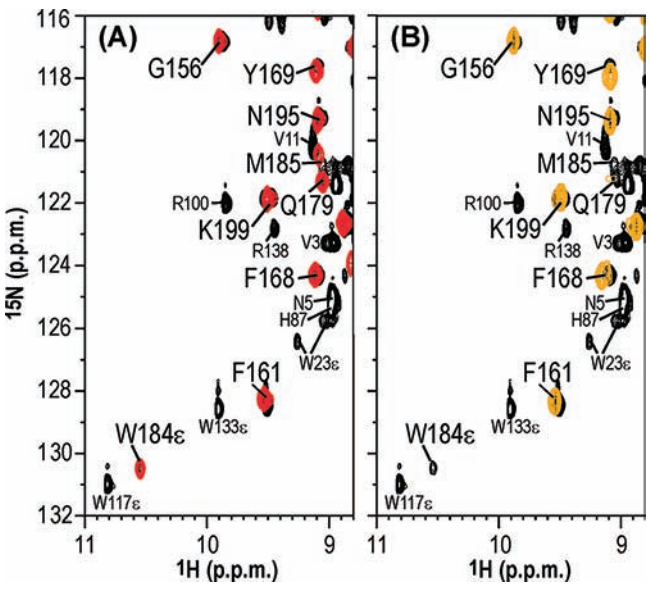

Figure 10. Superposition of selected regions of the 900 MHz ^{1}H−^{15}N HSQC spectra of CTD (144−231) (A, red) and CTD (150−231) (B, orange) and full-length CA (black). Spectra were recorded at 25 °C, pH 6.5, on 2.0 mM ^{15}N/^{13}C-labeled CTD (144−231), 2.6 mM ^{15}N/^{13}C-labeled CTD (150−231), and 0.87 mM ^{2}H/^{15}N/^{13}C-labeled full-length CA. Amide resonances of the CTDs and NTDs are labeled by residue names and numbers in large font and small font, respectively.

dx.doi.org/10.1021/ja300937v | J. Am. Chem. Soc. 2012, 134, 6455−6466

(150−231) (Figure 10A,B, respectively, and Figures S6 and S7 in the Supporting Information). Most of the resonances of CTD (144−231) (colored red in Figure 10A) are also observed in full-length CA (colored black in Figure 10A), at identical resonance frequencies. Therefore, it is most likely that the dimer interface that was observed in the structure of CTD (144−231) is also present in full length CA. In contrast, in the CTD (150−231) spectrum, resonances of residues at the dimer interface, for example, the W184 $N_{\varepsilon 1}H$ and M185 NH resonances, are missing (Figure 10B).

Distinct Dimer Conformations Can Be Frozen Out at Low Temperature. Species that undergo chemical exchange in the unfavorable intermediate exchange regime that is associated with severe line broadening may be observed if the exchange can be pushed into either the slow or the fast regime. For CTD (150−231), lowering the temperature from 25 to 7 °C (Figure 11A) resulted in resolution of individual resonances for two species: the W184 $N_{\varepsilon 1}H$ side-chain resonance as well as the backbone NH resonances of T186, E180, and Q179 resolved into two sets of signals. For example, the T186 amide

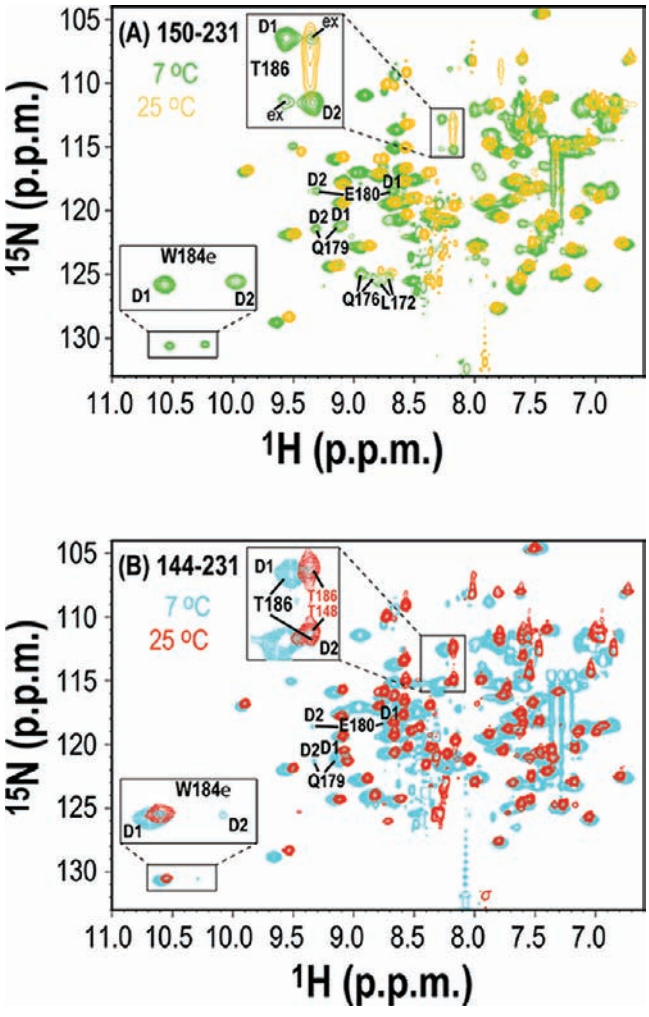

Figure 11. Superposition of 900 MHz $^{1}H-^{15}N$ HSQC spectra of the CTD at 25 and 7 °C. (A) $^{1}H-^{15}N$ HSQC spectra of CTD (150−231) at 25 °C (orange) and 7 °C (green). (B) $^{1}H-^{15}N$ HSQC spectra of CTD (144−231) at 25 °C (red) and 7 °C (cyan). The pH of the samples was 6.5. Resonances for the different dimer species are labeled as D1 and D2 and the exchange peaks from T186 of CTD (150−231) at 7 °C are labeled as "ex".

resonance that appears as a vertically trailing broad peak at 25 °C, clearly resolves into two separate resonances at 7 °C (labeled D1 and D2 in Figure 11A), that are connected by exchange cross peaks. The exchange rate between D1 and D2 is 140 s^{-1} (exchange time of ∼7 ms) (see Materials and Methods), and the two species are present in approximately equal amounts: the relative resonance intensities of the W184 $N_{\varepsilon 1}H$ side-chain and T186 NH backbone resonances yielded D1 and D2 fractions of 0.56 ± 0.03 and 0.44 ± 0.03, respectively (Figure 11A, Table 1). With respect to the quaternary state of the D1 and D2 species, it is very unlikely that the exchanging species are monomer and dimer, given that ∼95% of the protein should be dimeric at a protein concentration of 2.6 mM, based on the K_d value of 11.0 ± 7.6 μM for CTD (150−231). Nevertheless, we measured the relative resonance intensities for two additional protein concentrations, 1.0 mM and 0.50 mM, noting essentially identical intensity ratios for D1/D2 (0.60/0.40 and 0.55/0.45;Table 1). Therefore, both D1 and D2 are two different dimer conformers.

The $^{1}H-^{15}N$ HSQC spectrum of the longer CTD construct (144−231) at 7 °C also showed two species (W184 $N_{\varepsilon 1}H$ and T186, E180 and Q179 NH resonances are split into two; Figure 11B), and the chemical shifts of the D1 and D2 resonances for CTD (144−231) and CTD (150−231) are very similar: for example, (10.59/130.7 ppm) and (10.52/130.6 ppm) for the W184 $N_{\varepsilon 1}H$ resonance of D1 and (10.29/130.6 ppm) and (10.23/130.5 ppm) for D2. The same holds for the resonances of other interfacial residues such as Q179, E180 and T186 (Figure 11). However, the relative amounts of the two species are very different: in the longer CTD (144−231) the D1 conformer is by far the predominant species (93%) (Figure 11 and Table 1). This explains the dramatic difference in line broadening for CTD (144−231) and CTD (150−231) at 25 °C (Figure 9), with the D1 resonances of CTD (144−231) only weakly affected by exchange with the minor D2 form, while for the shorter CTD (150−231) the approximately equal amounts of the two forms, cause broadening of both sets of resonances by the exchange process.[65,66]

Similar to the observations for the two CTDs, the $^{1}H-^{15}N$ HSQC spectrum of full-length CA at 7 °C also exhibits multiple conformers (Figure 12 and Table 2), again most easily detected on the W184 $N_{\varepsilon 1}H$ resonance. Based on their resonance frequencies, the major (47%) and minor (16%) forms appear to be very similar to the D1 and D2 conformers of the CTD. Likewise, the E180 amide resonance frequencies in full-length CA and CTD (144−231) are very similar (Figure 12B), while chemical shifts of full-length CA and CTD (150−231) are less similar (Figure 12A), supporting the conclusion that full-length CA adopts a dimer structure that resembles more closely CTD (144−231) than CTD (150−231).

Interestingly, full-length CA adopts a third conformation (D3) whose side-chain W184 $N_{\varepsilon 1}H$ resonance position is similar, but not identical, to that observed for the major D1 conformer (Figure 12). The significant amount of the third conformer (37%) in full-length CA suggests that the proportions of the different conformers are easily modulated by experimental conditions, and that capsid assembly via dimerization of the CA-CTD can proceed through varied, but overall similar dimerization interfaces.

The Conformational Equilibrium Is Associated with Protonation of Glu-175. The equilibrium populations of the two main conformers, D1 and D2, differ dramatically between

dx.doi.org/10.1021/ja300937v | J. Am. Chem. Soc. 2012, 134, 6455−6466

Table 1. Fractions of D1 and D2 Conformers at 7 °C, Extracted from Peak Intensities in the 900 MHz $^{1}H-^{15}N$ HSQC Spectra of CTD (150−231) and CTD (144−231) Samples for Three Different Concentrations

CTD (150−231)			CTD (144−231)		
	D1	D2		D1	D2
W184ε (2.6 mM)	0.56	0.44	W184ε (2.5 mM)	0.91	0.09
T186 (2.6 mM)	0.52	0.48			
W184ε (1.0 mM)	0.62	0.38	W184ε (2.0 mM)	0.93	0.07
T186 (1.0 mM)	0.57	0.43			
W184ε (0.5 mM)	0.57	0.43	W184ε (0.44 mM)	0.93	0.07
T186 (0.5 mM)	0.54	0.46			
Average	0.56 ± 0.04	0.44 ± 0.04	Average	0.93 ± 0.01	0.07 ± 0.01

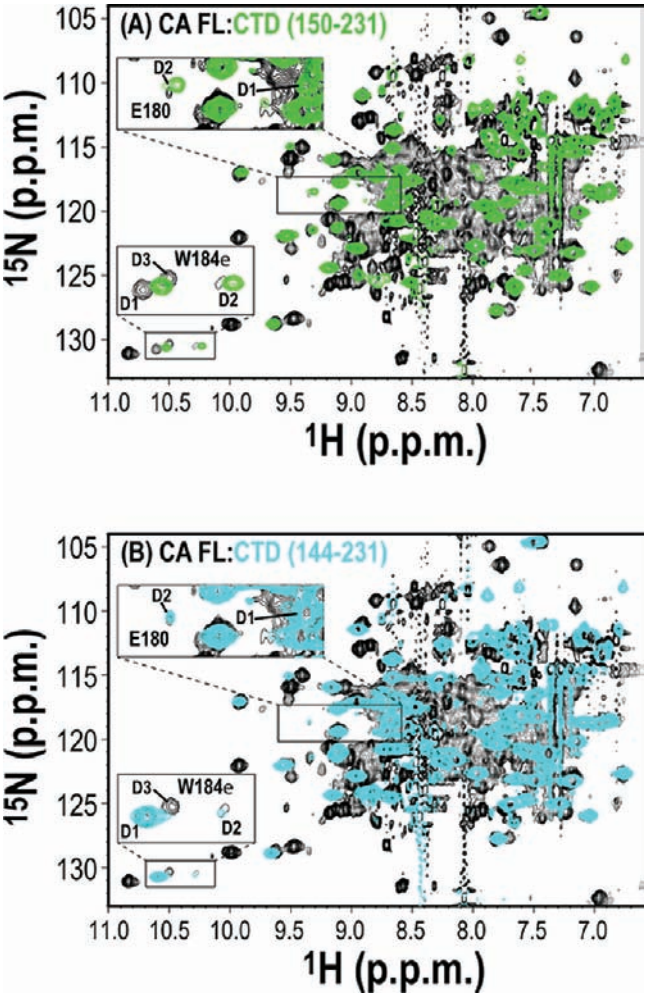

Figure 12. Superposition of 900 MHz $^{1}H-^{15}N$ HSQC spectra of CTD (150−231) (A) or CTD (144−231) (B) and full-length CA at 7 °C. Spectra were recorded on 2.6 mM $^{15}N/^{13}C$-labeled CTD (150−231) (green), 2.0 mM $^{15}N/^{13}C$-labeled CTD (144−231) (cyan) and 0.87 mM $^{2}H/^{15}N/^{13}C$-labeled full-length CA (black). The pH of the samples was 6.5. Resonances for the different dimer species are labeled with D1, D2, and D3.

CTD (150−231) and CTD (144−231), despite similar equilibrium dimerization constants. Since the conformational preferences of full-length CA are similar to those of the longer CTD (144−231), we reasoned that the removal of several hinge residues could perturb the CTD structure such, that different conformers around the dimer interface ensue. We therefore closely inspected the available CTD structures, namely 2KOD[13] (residues 144−231), 1A43[14] (residues 146−231), and 1A8O (residues 151−231). In 2KOD the side-chain O_{ε} atom of E175 of one subunit is close to W184 $H_{\varepsilon 1}$ of the other subunit (3.9 Å), while in 1A43 and 1A8O, these atoms are much further apart (6.7 and 7.4 Å, respectively). This suggested a possible role for the titratable E175 side chain. We therefore examined whether the different conformers exhibited any pH dependence, and found that the populations of the D1 and D2 conformers in CTD (144−231) are indeed dependent on pH, with the D1 fraction increasing from ∼0 at pH 4.0 to 0.91 at pH 6.5 and with the corresponding pK_a of 4.37 (Figure 13A). This pK_a is clearly compatible with a glutamate side chain, most likely E175 that is located at the dimer interface and in close proximity to W184 in our solution NMR structure of the CTD (144−231) (inset in Figure 13A). Naturally, the $^{1}H-^{15}N$ HSQC peak intensities and chemical shifts of the E175 NH backbone resonances also exhibit a strong pH dependence; however, no quantitative information could be extracted due to spectral overlap (see Supporting Information Figure S8). The D1 conformer, the predominant species at pH 6.5, corresponds to the structure in which W184 ($H_{\varepsilon 1}$) is interacting with the charged E175 (O_{ε}) side chain, while at low pH the minor conformer contains the E175 protonated side chain. Thus, E175 acts as a conformational switch by controlling, through its protonation state, the equilibrium populations of the two main dimer conformers. This conformational switching mechanism will also be operational in the full-length CA dimer in solution, since E175 and W184 are also located within a close range.

Table 2. Fractions of D1, D2, and D3 Conformers at 7 °C, Extracted from the W184 $N_{\varepsilon 1}H$ Resonance Intensities in the 900 MHz $^{1}H-^{15}N$ HSQC Spectra of 0.87 mM and 0.54 mM Full-Length CA

	D1	D2	D3
W184ε (0.87 mM)	0.47	0.16	0.37
W184ε (0.54 mM)	0.44	0.18	0.38
average	0.46 ± 0.01	0.17 ± 0.01	0.37 ± 0.01

In contrast, the relative populations of D1 and D2 in the short CTD (150−231) are pH-invariant (Figure 13B), in agreement with the structural findings in the crystallographic CTD (151−231) dimer (1A8O):[14] E175 is not close enough to W184 (W184 ($H_{\varepsilon 1}$) − E175 (O_{ε}) distance = 7.4 Å, inset in Figure 13B) to allow for a pH-dependent effect on the dimer conformation.

Biological Implications of Backbone Motions in the Hinge Region and Multiple CA Conformers. The observation of substantial conformational variability of the CA protein at the CTD dimer interface may be of significant importance in HIV-1 capsid assembly.[67,68] Structural plasticity of CA is required for assembly into hexamers and pentamers

dx.doi.org/10.1021/ja300937v | J. Am. Chem. Soc. 2012, 134, 6455−6466

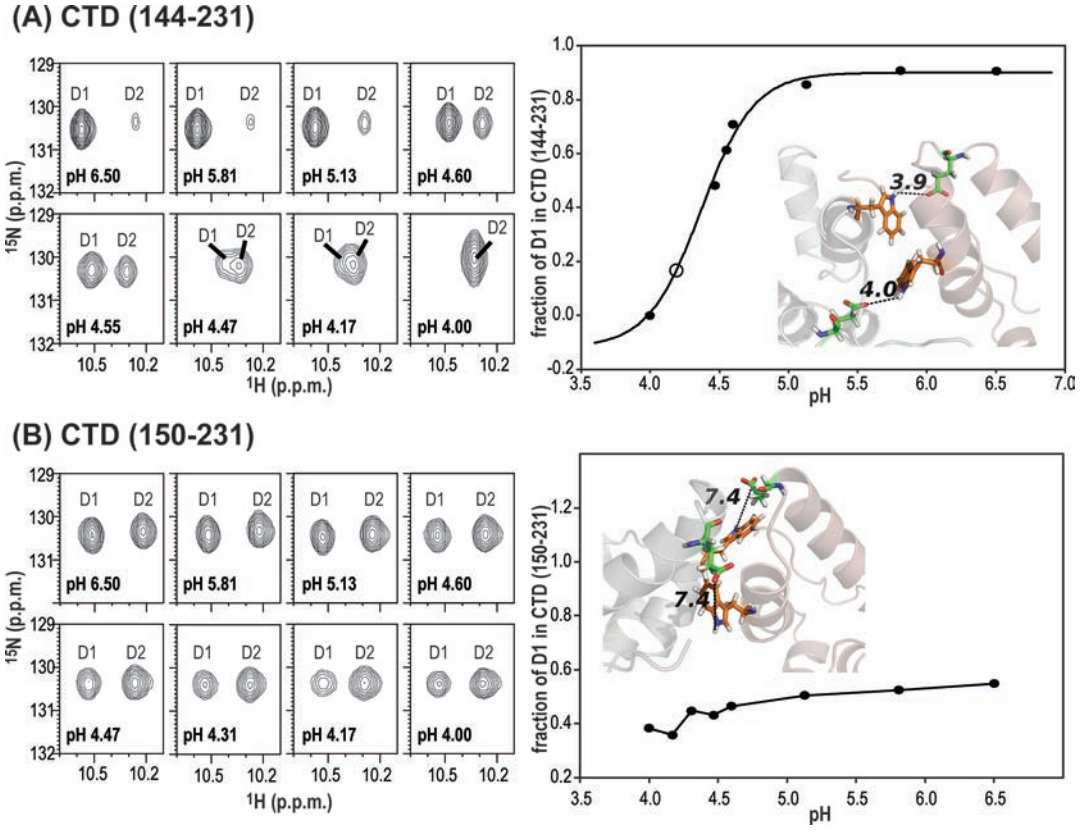

Figure 13. pH dependence of the W184 $H_{\varepsilon 1}N$ resonances of the D1 and D2 conformers. Expansion of the 600 MHz $^{1}H-^{15}N$ HSQC spectra of 2.5 mM CTD (144−231) (A, left) and 2.6 mM CTD (150−231) (B, left) for pH values ranging from 6.5 to 4.0, centered on the W184 resonance. In (A, right) and (B, right), the fraction of D1 (D1 peak height/(D1 peak height + D2 peak height)) is plotted against pH for CTD (144−231) and CTD (150−231), respectively. The experimental points are shown as circles. The fraction of D1 at pH 4.17 in (A, right) contains a large error due to severe overlap of D1 and D2 resonances and is marked with open circle. In (A, right), the line represents the fit of the experimental data to titration curve; the pK_a value derived from the fit is 4.37. Insets in (A, right) and (B, right), show ribbon diagrams of the CTD (144−231) 3D structure (NMR structure, PDB file 2KOD) and CTD (151−231) (X-ray structure, PDB file 1A8O). In the structures, one monomer unit is colored gray and the other pink; W184 and E175 residues are shown in stick representation, and the W184 ($H_{\varepsilon 1}$) − E175 ($O_{\varepsilon 2}$) distances are listed.

and into the capsid cone surface. This is enabled by millisecond time scale backbone motions of the hinge region, as evidenced by the solid-state NMR data for Y145. Indeed, slightly different intermolecular interfaces are required in HIV-1 capsid assembly in order to accommodate the non-uniform curvature of an ovoid,[7−10,12,13] and different oligomeric structures were used to built an overall model of the HIV capsid cone.[29]

Outlook and Future Directions. Our current data support the notion that conformational flexibility in the CA protein regulates the assembly of CA into multiple shapes, although much remains to be learned about the dynamic properties of assembled CA capsids in the context of uncoating and maturation. Here, we used tyrosines as probes for reporting on motional properties in the solid state. Future work that employs U-^{13}C,^{15}N-labeled CA will allow us to examine the dynamics of multiple residues over the entire protein in the assembled state and will inform about structural and dynamic details in capsid asssemblies.

CONCLUSIONS

Structural plasticity of HIV-1 CA is a necessary prerequisite for the protein's assembly into pleiomorphic capsid cones. MAS solid-state NMR data clearly revealed millisecond time scale motion of hinge region residues in CA, as exemplified for the pivotal residue Y145. While inherent backbone flexibility of CA opens up the available conformational space, the actual number of conformers accessible for CA assembly into varied morphologies is finite, and their relative populations in solution appear associated with an electrostatic interaction between the W184 and E175 side chains. The absence of key hinge residues, including Y145, results in loss of this interaction. Taken together, our solution and solid-state NMR results indicate that the ability to access multiple conformers through the hinge motion NTD and CTD, with the relative conformer populations controlled by intermolecular electrostatic interaction, permits the formation of varied capsid morphologies in mature HIV virions.

ASSOCIATED CONTENT

Supporting Information

Temperature dependence of the 600 MHz solid-state NCA spectra of full-length CA conical assemblies and CTD (142−231); 600 MHz $^{1}H-^{15}N$ HSQC spectra of CTD (150−231); 900 MHz $^{1}H-^{15}N$ HSQC spectra of U-$^{13}C/^{15}N$-labeled CTD (144−231), U-$^{13}C/^{15}N$-labeled CTD (150−231), U-$^{13}C/^{15}N$-labeled CTD (137−231), U-$^{13}C/^{15}N$-labeled CTD (142−231), U-$^{13}C/^{15}N$-labeled full-length CA, and U-$^{13}C/^{15}N$-tyrosine labeled full-length CA; as well as superpositions of the $^{1}H-^{15}N$ HSQC spectra of these proteins, highlighting resonances of the D1 and D2 conformers. This material is available free of charge via the Internet at http://pubs.acs.org.

dx.doi.org/10.1021/ja300937v | J. Am. Chem. Soc. 2012, 134, 6455−6466

AUTHOR INFORMATION

Corresponding Author

amg100@pitt.edu; tpolenov@udel.edu

Author Contributions

[⊥]These authors contributed equally to this publication.

Notes

The authors declare no competing financial interest.

ACKNOWLEDGMENTS

We thank Maria DeLucia and Jason Concel for expert technical assistance with protein preparations, Mike Delk for solution NMR support, and Dr. Verna Frasca for expert help with ITC data analysis. This work was supported by the National Institutes of Health (NIGMS Grant P50GM082251 and NCRR grants 5P30RR031160-03 and 8P30GM103519-03) and is a contribution from the Pittsburgh Center for HIV Protein Interactions.

REFERENCES

(1) Ashorn, P.; McQuade, T. J.; Thaisrivongs, S.; Tomasselli, A. G.; Tarpley, W. G.; Moss, B. *Proc. Natl. Acad. Sci. U.S.A.* **1990**, *87*, 7472.

(2) Barre-Sinoussi, F.; Chermann, J. C.; Rey, F.; Nugeyre, M. T.; Chamaret, S.; Gruest, J.; Dauguet, C.; Axler-Blin, C.; Vezinet-Brun, F.; Rouzioux, C.; Rozenbaum, W.; Montagnier, L. *Science* **1983**, *220*, 868.

(3) Campbell, S.; Vogt, V. M. *J. Virol.* **1995**, *69*, 6487.

(4) Gallo, R. C.; Salahuddin, S. Z.; Popovic, M.; Shearer, G. M.; Kaplan, M.; Haynes, B. F.; Palker, T. J.; Redfield, R.; Oleske, J.; Safai, B.; White, G.; Foster, P.; Markham, P. D. *Science* **1984**, *224*, 500.

(5) Gottlinger, H. G.; Sodroski, J. G.; Haseltine, W. A. *Proc. Natl. Acad. Sci. U.S.A.* **1989**, *86*, 5781.

(6) Kohl, N. E.; Emini, E. A.; Schleif, W. A.; Davis, L. J.; Heimbach, J. C.; Dixon, R. A.; Scolnick, E. M.; Sigal, I. S. *Proc. Natl. Acad. Sci. U.S.A.* **1988**, *85*, 4686.

(7) Benjamin, J.; Ganser-Pornillos, B. K.; Tivol, W. F.; Sundquist, W. I.; Jensen, G. J. *J. Mol. Biol.* **2005**, *346*, 577.

(8) Briggs, J. A.; Grunewald, K.; Glass, B.; Forster, F.; Krausslich, H. G.; Fuller, S. D. *Structure* **2006**, *14*, 15.

(9) Briggs, J. A.; Wilk, T.; Welker, R.; Krausslich, H. G.; Fuller, S. D. *EMBO J.* **2003**, *22*, 1707.

(10) Welker, R.; Hohenberg, H.; Tessmer, U.; Huckhagel, C.; Krausslich, H. G. *J. Virol.* **2000**, *74*, 1168.

(11) Ganser, B. K.; Li, S.; Klishko, V. Y.; Finch, J. T.; Sundquist, W. I. *Science* **1999**, *283*, 80.

(12) Li, S.; Hill, C. P.; Sundquist, W. I.; Finch, J. T. *Nature* **2000**, *407*, 409.

(13) Byeon, I. J.; Meng, X.; Jung, J.; Zhao, G.; Yang, R.; Ahn, J.; Shi, J.; Concel, J.; Aiken, C.; Zhang, P.; Gronenborn, A. M. *Cell* **2009**, *139*, 780.

(14) Gamble, T. R.; Yoo, S.; Vajdos, F. F.; von Schwedler, U. K.; Worthylake, D. K.; Wang, H.; McCutcheon, J. P.; Sundquist, W. I.; Hill, C. P. *Science* **1997**, *278*, 849.

(15) Newman, J. L.; Butcher, E. W.; Patel, D. T.; Mikhaylenko, Y.; Summers, M. F. *Protein Sci.* **2004**, *13*, 2101.

(16) Tang, C.; Ndassa, Y.; Summers, M. F. *Nat. Struct. Biol.* **2002**, *9*, 537.

(17) Gamble, T. R.; Vajdos, F. F.; Yoo, S.; Worthylake, D. K.; Houseweart, M.; Sundquist, W. I.; Hill, C. P. *Cell* **1996**, *87*, 1285.

(18) Gitti, R. K.; Lee, B. M.; Walker, J.; Summers, M. F.; Yoo, S.; Sundquist, W. I. *Science* **1996**, *273*, 231.

(19) Momany, C.; Kovari, L. C.; Prongay, A. J.; Keller, W.; Gitti, R. K.; Lee, B. M.; Gorbalenya, A. E.; Tong, L.; McClure, J.; Ehrlich, L. S.; Summers, M. F.; Carter, C.; Rossmann, M. G. *Nat. Struct. Biol.* **1996**, *3*, 763.

(20) Ivanov, D.; Tsodikov, O. V.; Kasanov, J.; Ellenberger, T.; Wagner, G.; Collins, T. *Proc. Natl. Acad. Sci. U.S.A.* **2007**, *104*, 4353.

(21) Ternois, F.; Sticht, J.; Duquerroy, S.; Krausslich, H. G.; Rey, F. A. *Nat. Struct. Mol. Biol.* **2005**, *12*, 678.

(22) Worthylake, D. K.; Wang, H.; Yoo, S.; Sundquist, W. I.; Hill, C. P. *Acta Crystallogr. D Biol. Crystallogr.* **1999**, *55*, 85.

(23) Du, S.; Betts, L.; Yang, R.; Shi, H.; Concel, J.; Ahn, J.; Aiken, C.; Zhang, P.; Yeh, J. I. *J. Mol. Biol.* **2011**, *406*, 371.

(24) Berthet-Colominas, C.; Monaco, S.; Novelli, A.; Sibai, G.; Mallet, F.; Cusack, S. *EMBO J.* **1999**, *18*, 1124.

(25) Ganser-Pornillos, B. K.; Cheng, A.; Yeager, M. *Cell* **2007**, *131*, 70.

(26) Alcaraz, L. A.; del Alamo, M.; Mateu, M. G.; Neira, J. L. *FEBS J.* **2008**, *275*, 3299.

(27) Shin, R.; Tzou, Y. M.; Krishna, N. R. *Biochemistry* **2011**, *50*, 9457.

(28) Wong, H. C.; Shin, R.; Krishna, N. R. *Biochemistry* **2008**, *47*, 2289.

(29) Pornillos, O.; Ganser-Pornillos, B. K.; Yeager, M. *Nature* **2011**, *469*, 424.

(30) Pornillos, O.; Ganser-Pornillos, B. K.; Kelly, B. N.; Hua, Y.; Whitby, F. G.; Stout, C. D.; Sundquist, W. I.; Hill, C. P.; Yeager, M. *Cell* **2009**, *137*, 1282.

(31) Jiang, J.; Ablan, S. D.; Derebail, S.; Hercik, K.; Soheilian, F.; Thomas, J. A.; Tang, S.; Hewlett, I.; Nagashima, K.; Gorelick, R. J.; Freed, E. O.; Levin, J. G. *Virology* **2011**, *421*, 253.

(32) Chevelkov, V.; Fink, U.; Reif, B. *J. Biomol. NMR* **2009**, *45*, 197.

(33) Giraud, N.; Blackledge, M.; Goldman, M.; Bockmann, A.; Lesage, A.; Penin, F.; Emsley, L. *J. Am. Chem. Soc.* **2005**, *127*, 18190.

(34) Krushelnitsky, A.; Reichert, D. *Prog. Nucl. Magn. Reson. Spectrosc.* **2005**, *47*, 1.

(35) Yang, J.; Tasayco, M. L.; Polenova, T. *J. Am. Chem. Soc.* **2009**, *131*, 13690.

(36) Erickson-Viitanen, S.; Manfredi, J.; Viitanen, P.; Tribe, D. E.; Tritch, R.; Hutchison, C. A. III; Loeb, D. D.; Swanstrom, R. *AIDS Res. Hum. Retroviruses* **1989**, *5*, 577.

(37) Sun, S.; Han, Y.; Paramasivam, S.; Yan, S.; Siglin, A. E.; Williams, J. C.; Byeon, I. J.; Ahn, J.; Gronenborn, A. M.; Polenova, T. *Methods Mol. Biol.* **2012**, *831*, 303.

(38) Bello, M.; Perez-Hernandez, G.; Fernandez-Velasco, D. A.; Arreguin-Espinosa, R.; Garcia-Hernandez, E. *Proteins* **2008**, *70*, 1475.

(39) Burrows, S. D.; Doyle, M. L.; Murphy, K. P.; Franklin, S. G.; White, J. R.; Brooks, I.; McNulty, D. E.; Scott, M. O.; Knutson, J. R.; Porter, D.; Young, P. R.; Hensley, P. *Biochemistry* **1994**, *33*, 12741.

(40) van Geet, A. L. *Anal. Chem.* **1968**, *40*, 2227.

(41) Bax, A.; Grzesiek, S. *Acc. Chem. Res.* **1993**, *26*, 131.

(42) Clore, G. M.; Gronenborn, A. M. *Trends Biotechnol.* **1998**, *16*, 22.

(43) Pascal, S. M.; Muhandiram, D. R.; Yamazaki, T.; Formankay, J. D.; Kay, L. E. *J. Magn. Reson. Ser. B* **1994**, *103*, 197.

(44) Sattler, M.; Maurer, M.; Schleucher, J.; Griesinger, C. *J. Biomol. NMR* **1995**, *5*, 97.

(45) Ernst, R. R.; Bodenhausen, G.; Wokaun, A. *Principles of Nuclear Magnetic Resonance in One and Two Dimensions*; Clarendon Press: Oxford, 1987; Vol. *14*, p 492.

(46) Markley, J. L. *Acc. Chem. Res.* **1975**, *8*, 70.

(47) Delaglio, F.; Grzesiek, S.; Vuister, G. W.; Zhu, G.; Pfeifer, J.; Bax, A. *J. Biomol. NMR* **1995**, *6*, 277.

(48) Goddard, T. D.; Kneller, D. G.; 3.110 ed.; University of California: San Francisco, 2004.

(49) Johnson, B. A.; Blevins, R. A. *J. Biomol. NMR* **1994**, *4*, 603.

(50) Han, Y.; Ahn, J.; Concel, J.; Byeon, I. J. L.; Gronenborn, A. M.; Yang, J.; Polenova, T. *J. Am. Chem. Soc.* **2010**, *132*, 1976.

(51) Neue, G.; Dybowski, C. *Solid State Nucl. Magn. Reson.* **1997**, *7*, 333.

(52) Morcombe, C. R.; Zilm, K. W. *J. Magn. Reson.* **2003**, *162*, 479.

(53) Hou, G. J.; Yan, S.; Sun, S. J.; Han, Y.; Byeon, I. J. L.; Ahn, J.; Concel, J.; Samoson, A.; Gronenborn, A. M.; Polenova, T. *J. Am. Chem. Soc.* **2011**, *133*, 3943.

(54) Takegoshi, K.; Nakamura, S.; Terao, T. *Chem. Phys. Lett.* **2001**, *344*, 631.

(55) Baldus, M.; Petkova, A. T.; Herzfeld, J.; Griffin, R. G. *Mol. Phys.* **1998**, *95*, 1197.
(56) Munowitz, M.; Aue, W. P.; Griffin, R. G. *J. Chem. Phys.* **1982**, *77*, 1686.
(57) Zhao, X.; Eden, M.; Levitt, M. H. *Chem. Phys. Lett.* **2001**, *342*, 353.
(58) Chan, J. C. C.; Tycko, R. *J. Chem. Phys.* **2003**, *118*, 8378.
(59) Gullion, T.; Schaefer, J. *J. Magn. Reson.* **1989**, *81*, 196.
(60) Bak, M.; Rasmussen, J. T.; Nielsen, N. C. *J. Magn. Reson.* **2000**, *147*, 296.
(61) Cheng, V. B.; Suzukawa, H. H.; Wolfsber, M. *J. Chem. Phys.* **1973**, *59*, 3992.
(62) Haeberlen, U. In *Advances in Magnetic Resonance*; Waugh, J. S., Ed.; Academic Press: Orlando, 1976; Vol. Supplement 1.
(63) Jung, J.; Byeon, I. J. L.; Ahn, J.; Concel, J.; Gronenborn, A. M. *Biomol. NMR Assign.* **2010**, *4*, 21.
(64) Bosco, D. A.; Kern, D. *Biochemistry* **2004**, *43*, 6110.
(65) Millet, O.; Loria, J. P.; Kroenke, C. D.; Pons, M.; Palmer, A. G. *J. Am. Chem. Soc.* **2000**, *122*, 2867.
(66) Tollinger, M.; Skrynnikov, N. R.; Mulder, F. A.; Forman-Kay, J. D.; Kay, L. E. *J. Am. Chem. Soc.* **2001**, *123*, 11341.
(67) Cardone, G.; Purdy, J. G.; Cheng, N.; Craven, R. C.; Steven, A. C. *Nature* **2009**, *457*, 694.
(68) Hyun, J. K.; Radjainia, M.; Kingston, R. L.; Mitra, A. K. *J. Biol. Chem.* **2010**, *285*, 15056.